ELSEVIER

J. Non-Newtonian Fluid Mech., 57 (1995) 227–241

Journal of Non-Newtonian Fluid Mechanics

Stability of two-layer Poiseuille flow of Carreau–Yasuda and Bingham-like fluids

A. Pinarbasi, A. Liakopoulos *

Department of Mechanical Engineering and Mechanics, Lehigh University, Bethlehem, PA 18015-3085, USA

Received 4 August 1994; in revised form 10 October 1994

Abstract

In this paper we present the linear stability analysis of the interface between two non-Newtonian inelastic fluids in a straight channel driven by a pressure gradient. Two rheological models of non-Newtonian behavior are studied: (a) Bingham-like fluids and (b) Carreau–Yasuda fluids. For each rheological model, the linearized equations describing the evolution of small two-dimensional disturbances are derived and the stability problem is formulated as an eigenvalue problem for a set of ordinary differential equations of the Orr–Sommerfeld type. Discretization is performed using a pseudospectral technique based on Chebyshev polynomial expansions. The resulting generalized matrix eigenvalue problem is solved using the QZ algorithm. The results on the onset of instability are presented in the form of stability maps for a range of zero-shear-rate viscosity ratios, thickness ratios, power-law constants, material time constants, Yasuda constants, apparent yield stresses and stress growth exponents. Increasing the stress growth exponents or apparent yield stresses of the viscoplastic fluids has a stabilizing effect on the interface. For shear thinning fluids, increasing the zero-shear-rate viscosity ratio or shear thinning of the fluids destabilizes the interface. The effect of other parameters can be stabilizing or destabilizing depending on the flow configuration and wavelength.

Keywords: Bingham-like fluids; Carreau–Yasuda fluids; Inelastic fluids; Poiseuille flow

1. Introduction

The study of instabilities in multilayer flows of immiscible, non-Newtonian fluids has received much attention in recent years mainly because of its relevance to the

* Corresponding author.

SSDI 0377-0257(94)01330-6

stability of coextrusion processes. Coextrusion processes are extensively used in the production of bilayer and multilayer films, sheets and pipes in the plastics industry, the concentric coating of two or more polymers and the production of conjugate fibers in the fiber industry. The popularity of multilayer extrusion has increased due to its ability to produce composite products with tailor-made properties. The coextrusion operation consists essentially of combining several melt streams in a feedblock. The combined melt stream then flows to the die where the layers take their final dimensions. In all coextrusion operations the rate of production is limited by the flow instabilities and especially instabilities at the interfaces between adjacent layers. These instabilities result in high scrap rates or final products with substandard mechanical, optical or barrier properties. Complete understanding of the physical origins of interfacial instability in coextrusion is the foremost step towards achieving high production rates together with improved product quality.

Since the early experimental results of Charles and Lilleleht [1], Yu and Sparrow [2], Kao and Park [3], and the theoretical analysis of Yih [4], it is known that viscosity stratification can cause instability. This instability depends on the wavenumber of the flow disturbance, a number of flow configuration parameters, e.g. depth ratios, and the viscosity ratios of the fluids involved. The stability analysis of steady, multi-layer, Newtonian internal flows has been largely confined to Couette, Poiseuille, and Couette–Poiseuille flows by numerical methods, short wave asymptotics and long wave asympototics (Yih [4]; Hickox [5]; Nakaya and Hasegawa [6]; Hooper and Boyd [7]; Hooper and Grimshaw [8]; Renardy [9–11]; and Yiantsios and Higgins [12]). From the practical point of view these studies suggest that in order to achieve linearly stable flow in the absence of density stratification, one should place the less viscous fluid in a thin layer (to stabilize long waves) and provide enough interfacial tension (to stabilize short waves). For the case of simultaneous viscosity and density stratification the above rule of thumb does not hold [11].

The importance of maintaining stable interfaces during coextrusion of polymeric liquids has led to the study of multi-layer non-Newtonian fluid flows. Li [13] studied the stability of two constant viscosity Oldroyd B fluids in plane Couette flow while Waters and Keeley [14] studied the case of power-law fluids and four-constant Oldroyd fluids. Renardy [15] considered Couette flow of two Maxwell fluids. Stability analysis of plane Poiseuille flow of two second order fluids has been presented by Khan and Han [16] and by Khomami [17]. More recently, the effects of shear thinning and elasticity in multi-layer plane Poiseuille flow were investigated by Su and Khomami [18,19] for power-law, second order and Oldroyd B fluids, and by Anturkar et al. [20] for Oldroyd B fluids with shear dependent viscosity described by the Carreau model. These authors found that shear thinning and elasticity stabilize or destabilize the interface depending on the disturbance wavelength and geometric configuration.

In this paper we present the linear stability analysis of the interface between two non-Newtonian, inelastic fluids in a straight channel (flat coextrusion die) driven by a pressure gradient acting along the channel centerline. Two rheological models of non-Newtonian behavior are studied: Bingham-like fluids and Carreau–Yasuda

fluids. The Bingham model has been used to describe the behavior of lubricants, in particular greases, as well as the flow of melts and slurries in molds and chemical processes. The Carreau–Yasuda model has been proven to be successful in describing the behavior of many polymer solutions and melts. It fits accurately many experimental viscosity curves over a wide range of shear rate. For each rheological model, the linearized equations describing the evolution of small disturbances are derived and the stability problem is formulated as an eigenvalue problem for a set of ordinary differental equations of the Orr–Sommerfeld type. Discretization is performed using a pseudospectral technique based on Chebyshev polynomial expansions. The resulting generalized matrix eigenvalue problem is solved using the QZ algorithm.

2. Governing equations

The flow geometry considered in this study is shown in Fig. 1. We examine the stability of the interface between two immiscible inelastic fluids flowing steadily in a straight channel. The continuity and momentum equations for each fluid layer can be expressed in dimensional form as

$$\frac{\partial \bar{u}_i^k}{\partial \bar{x}_i} = 0, \tag{1}$$

$$\bar{\rho}_k \left(\frac{\partial \bar{u}_j^k}{\partial \bar{t}} + \bar{u}_i^k \frac{\partial \bar{u}_j^k}{\partial \bar{x}_i} \right) = -\frac{\partial \bar{p}^k}{\partial \bar{x}_j} + \frac{\partial \bar{\tau}_{ij}^k}{\partial \bar{x}_i} \qquad j = 1,2. \tag{2}$$

Two inelastic fluid models are considered in this study: the Carreau Yasuda [21] (CY) and the Bingham-like [22] (BL) with constitutive equations

$$\bar{\tau}_{ij}^k = \bar{\mu}_k [1 + (\bar{\lambda}_k \dot{\bar{\gamma}}^k)^{a_k}]^{n_k - 1} \dot{\bar{\gamma}}_{ij}^k \qquad \text{(CY)}, \tag{3}$$

$$\bar{\tau}_{ij}^k = \bar{\mu}_k \left[1 + \frac{\bar{\tau}_y^k (1 - e^{-\bar{\mu}_k \dot{\bar{\gamma}}^k})}{\bar{\mu}_k \dot{\bar{\gamma}}^k} \right] \dot{\bar{\gamma}}_{ij}^k \qquad \text{(BL)}. \tag{4}$$

In the equations above, the summation convention is used over index i while k denotes the layer number. In addition, $\bar{\rho}_k$ and $\bar{\mu}_k$ are the density and zero-shear-rate viscosity of the kth layer, $\bar{p}$ is the pressure, $\bar{u}_i$ is the ith component of the velocity vector and $\bar{\tau}_{ij}$ *is the* (i,j)th component of the deviatoric stress tensor. In the constitutive equations,

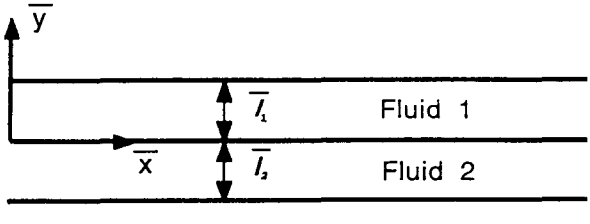

Fig. 1. Schematic diagram of flow domain.

$$\bar{\dot{\gamma}}_{ij} = \frac{\partial \bar{u}_i}{\partial \bar{x}_j} + \frac{\partial \bar{u}_j}{\partial \bar{x}_i}$$

is the (i,j)th component of the strain rate tensor, $\bar{\dot{\boldsymbol{\gamma}}}$; $\bar{\dot{\gamma}} = (0.5\bar{\pi}_{\dot{\gamma}})^{1/2}$ and $\bar{\pi}_{\dot{\gamma}}$ are the magnitude and the second invariant of the strain rate tensor, respectively. The three parameters in the CY model are the material time constant $\bar{\lambda}$, dimensionless power-law index n and the dimensionless constant a which describes the transition region between the zero-shear-rate region and the power-law region. The two parameters of the BL model are the apparent yield stress, $\bar{\tau}_y$ and the stress growth exponent, $\bar{h}$.

The governing equations are non-dimensionalized by using the interface velocity, $\bar{U}_0$, as reference velocity and the thickness of the upper layer, $\bar{l}_1$, as characteristic length, i.e.,

$$u_i = \frac{\bar{u}_i}{\bar{U}_0}, \qquad x_i = \frac{\bar{x}_i}{\bar{l}_1}, \qquad m_k = \frac{\bar{\mu}_k}{\bar{\mu}_1}, \qquad r_k = \frac{\bar{\rho}_k}{\bar{\rho}_1},$$

$$(t,\lambda,h) = \frac{(\bar{t},\bar{\lambda},\bar{h})\bar{U}_0}{\bar{l}_1}, \qquad (\boldsymbol{\tau},\tau_y,p) = \frac{(\bar{\boldsymbol{\tau}},\bar{\tau}_y,\bar{p})\bar{l}_1}{\bar{\mu}_1 \bar{U}_0}.$$

The governing equations in dimensionless form become

$$\frac{\partial u_i^k}{\partial x_j} = 0, \tag{5}$$

$$Re r_k \left(\frac{\partial u_j^k}{\partial t} + u_i^k \frac{\partial u_j^k}{\partial x_i} \right) = -\frac{\partial p^k}{\partial x_j} + \frac{\partial \tau_{ij}^k}{\partial x_i} \qquad j = 1,2, \tag{6}$$

$$\tau_{ij}^k = m_k [1 + (\lambda_k \dot{\gamma}^k)^{a_k}]^{n_k - 1/a_k} \dot{\gamma}_{ij}^k \qquad \text{(CY model)}, \tag{7}$$

$$\tau_{ij}^k = m_k \left[1 + \frac{\tau_y^k (1 - e^{-h_k \dot{\gamma}^k})}{m_k \dot{\gamma}^k} \right] \dot{\gamma}_{ij}^k \qquad \text{(BL model)}, \tag{8}$$

where m_k is the zero-shear-rate viscosity ratio, r_k is the density ratio, both for the kth layer, and the Reynolds number, Re, is defined as $Re = \bar{\rho}_1 \bar{U}_0 \bar{l}_1 / \bar{\mu}_1$.

2.1. Base flow

The undisturbed base flow is assumed to be fully developed and parallel. Therefore, the non-zero components of the deviatoric stress tensor take the dimensionless form (after switching from indicial notation i,j to conventional x,y notation)

$$\tau_{xy}^k = m_k (1 + \lambda_k^{a_k} |u'_{bk}|^{a_k})^{n_k - 1/a_k} u'_{bk} \qquad \text{(CY model)}, \tag{9}$$

$$\tau_{xy}^k = m_k \left[1 + \frac{\tau_y^k (1 - e^{-h_k |u'_{bk}|})}{m_k |u'_{bk}|} \right] u'_{bk} \qquad \text{(BL model)}, \tag{10}$$

where u_{bk} denotes the base velocity of the kth layer and primes denote differentiation with respect to y.

Since the interface of the base flow is flat, the pressure gradient along the channel is constant and uniform for both layers. Therefore, the x-component of the momentum equation, Eq. (6), reduces to

$$\frac{\partial \tau_{xy}^k}{\partial y} = G,$$

where $G = \mathrm{d}p/\mathrm{d}x$ is the dimensionless pressure gradient and the shear stress distribution is given by

$$\tau_{xy}^k = Gy + c_k \qquad k = 1,2. \tag{11}$$

The base flow velocity distributions are obtained by combining Eqs. (11) and (9) for the CY model

$$m_k (1 + \lambda_k^{a_k} |u'_{bk}|^{a_k})^{n_k - 1/a_k} u'_{bk} = Gy + c_k, \qquad k = 1,2, \tag{12}$$

and Eqs. (11) and (10) for the BL model

$$m_k \left[1 + \frac{\tau_y^k (1 - \mathrm{e}^{b_k |u_{bk}|})}{m_k |u'_{bk}|} \right] u'_{bk} = Gy + c_k, \qquad k = 1,2. \tag{13}$$

The associated boundary conditions (no-slip at the channel walls and continuity of velocity and shear stress at the interface) are expressed in dimensionless form by

$$u_{b1}(1) = u_{b2}(-\varepsilon) = 0, \tag{14a}$$

$$u_{b1}(0) = u_{b2}(0) = 1, \tag{14b}$$

$$\tau_{xy_1}(0) = \tau_{xy_2}(0), \tag{14c}$$

where $\varepsilon = \bar{l}_2/\bar{l}_1$ denotes the layer thickness ratio.

Differential Eqs. (12) and (13), along with the boundary conditions (14a)–(14c), determine the base-flow velocity profiles for CY and BL fluids, respectively. The two boundary-value problems are solved numerically using a Chebyshev-pseudospectral method [23,24]. After transforming the domain of each layer to $-1 \le Y \le 1$, u_{bk} is discretized in Y and expanded in a series of Chebyshev polynomials of the first kind $T_n(Y)$, defined as $T_n(\cos\theta) = \cos(n\theta)$. Truncating the series after N terms results in a set of non-linear algebraic equations with $2(N+2)$ unknowns which is solved using the routine *hybrj* of minpack. Further details on the application of Chebyshev-pseudospectral methods to the problem at hand are given by Pinarbasi and Liakopoulos [25].

2.2. Linear stability analysis

The velocity and stress fields are perturbed by imposing two-dimensional infinitesimal disturbances on the base flow, i.e.

$$\begin{aligned} u_k(x,y,t) &= u_{bk}(y) + \hat{u}_k(x,y,t), \\ v_k(x,y,t) &= \hat{v}_k(x,y,t), \end{aligned} \tag{15}$$

$$p_k(x,y,t) = p_{bk}(x) + \hat{p}_k(x,y,t),$$

$$\tau_k(x,y,t) = \tau_{bk}(y) + \hat{\tau}_k(x,y,t).$$

Disturbance equations are derived by substitution of Eqs. (15) into Eqs. (5) and (6), subtraction of the base flow equations, and linearization.

The continuity equation for the disturbances is satisfied by introducing a perturbation streamfunction, $\hat{\psi}_k$, for each layer, i.e.

$$\hat{u}_k = \frac{\partial \hat{\psi}_k}{\partial y}, \qquad \hat{v}_k = -\frac{\partial \hat{\psi}_k}{\partial x}, \qquad k = 1,2.$$

It is further assumed that all disturbances have time and spatial dependence [26] of the form,

$$(\hat{\psi}_k, \hat{p}_k, \hat{\tau}_k) = [\phi_k(y), f_k(y), s_k(y)]e^{i\alpha(x-ct)}, \qquad k = 1,2, \tag{16}$$

where α is the wave number (real and positive), $c = c_r + ic_i$ is the complex velocity and ϕ_k, f_k, s_k denote the spatially-varying disturbance amplitudes. The sign of c_i determines the stability of the flow, i.e., if $c_i > 0$ the flow is temporally unstable.

Substituting Eq. (16) into the linearized momentum equations and eliminating pressure perturbations by cross-differentiation, the stability governing equations become

$$i\alpha Re_k[(u_{bk} - c)(\phi_k'' - \alpha^2\phi_k) - u_{bk}''\phi_k]$$
$$= s_{xy_k}'' + \alpha^2 s_{xy_k} + i\alpha(s_{xx_k}' - s_{yy_k}'), \qquad k = 1,2 \text{ (no summation)}, \tag{17}$$

where primes denote derivatives with respect to y and s_{xx}, s_{yy}, s_{xy} are the amplitudes of the perturbation stress tensor components. The associated boundary conditions are:

No slip at solid walls

$$\phi_1 = \phi_1' = 0 \text{ at } y = 1,$$

$$\phi_2 = \phi_2' = 0 \text{ at } y = -\varepsilon. \tag{18a}$$

Continuity of velocities at the fluid–fluid interface ($y = 0$)

$$\phi_1 = \phi_2\ ; \qquad \phi_1' - \phi_2' = \frac{\phi_1}{c - u_{b1}}(u_{b2}' - u_{b1}'). \tag{18b}$$

Continuity of shear stress at the fluid–fluid interface ($y = 0$)

$$s_{xy_1} = s_{xy_2} \tag{18c}$$

Continuity of normal stress at the fluid–fluid interface ($y = 0$)

$$i\alpha Re[(u_{b1} - c)\phi_1' - u_{b1}'\phi_1] - i\alpha Re r_2[(u_{b2} - c)\phi_2' - u_{b2}'\phi_2] + i\alpha(s_{xx} - s_{yy})_2$$
$$- i\alpha(s_{xx} - s_{yy})_1 + (s_{xy}')_2 - (s_{xy}')_1 = i\alpha(F + \alpha^2 S)\frac{\phi_1}{c - u_{b1}}, \tag{18d}$$

where $S = \bar{T}/(\bar{\mu}_1 \bar{U}_0)$ and $F = (\bar{\rho}_2 - \bar{\rho}_1)\bar{g}\bar{l}_1^2/(\bar{\mu}_1 \bar{U}_0)$ are dimensionless groups accounting for the effects of interfacial tension, $\bar{T}$, and the gravitational acceleration, g.

Upon substitution of Eq. (16) into the dimensionless constitutive equations and neglecting non-linear terms, the expressions for the amplitudes of the perturbation stress tensor components become

$$s_{xy_k} = 2i\alpha\eta_k(y)\phi_k', \tag{19a}$$

$$s_{yy_k} = -2i\alpha\eta_k(y)\phi_k', \tag{19b}$$

$$s_{xy_k} = \beta_k(y)(\phi_k'' + \alpha^2\phi_k), \tag{19c}$$

$k = 1,2$ (no summation), where

$$\eta_k(y) = m_k(1 + \lambda_k^{a_k}|u_{bk}'|^{a_k})^{n_k - 1/a_k}, \tag{20a}$$

$$\beta_k(y) = \eta_k(y)\left[1 + \frac{(n_k - 1)\lambda_k^{a_k}|u_{bk}'|^{a_k}}{1 + \lambda_k^{a_k}|u_{bk}'|^{a_k}}\right] \tag{20b}$$

for the CY model, and

$$\eta_k(y) = m_k\left[1 + \frac{\tau_y^k}{m_k|u_{bk}'|}(1 - e^{-h_k|u_{bk}'|})\right], \tag{21a}$$

$$\beta_k(y) = m_k\left(1 + \frac{\tau_y^k h_k}{m_k} e^{-h_k|u_{bk}'|}\right) \tag{21b}$$

for the BL model.

Substitution of Eqs. (19) into Eqs. (17) and (18) results in a formulation in terms of ϕ_k, c and α, with the dimensionless Π-groups as parameters. In this paper, we approach the stability question as a temporal stability problem, i.e. for an arbitrary positive real value of α, we seek solutions to the resulting eigenanalysis problem and obtain the complex eigenvalue c and the corresponding eigenfunction ϕ_k.

3. Method of solution

The continuous eigenvalue problem formulated in the previous section is discretized using a pseudospectral method. After appropriate coordinate transformations (see below), the functions ϕ_k, $k = 1,2$, are expanded in series of Chebyshev polynomials. Truncating each series after N terms, $N+1$ expansion coefficients are introduced as unknowns in each layer. Eqs. (17) are discretized at $N-3$ collocation points in each layer given by

$$Y_j = \cos\left(\frac{\pi j}{N-4}\right) \qquad j = 0, 1, 2, \ldots, N-4.$$

These $2N-6$ equations are supplemented by the eight boundary conditions, Eq. (18), to obtain $2(N+1)$ equations. This procedure results in a generalized algebraic eigenvalue problem of the form $Ax = cBx$ which is solved using *dgvlcg*, an *IMSL*

Table 1
Comparison of asymptotic and numerical results for two Newtonian fluids

m_2	α	Asymptotic (Yih [4])	Numerical, present study (CY, $n_1 = n_2 = 1$)	Numerical, present study (BL, $\tau_{y1} = \tau_{y2} = 0$)
10	1×10^{-5}	$1.67219 + i1.24810 \times 10^{-6}$	$1.67219 + i1.24802 \times 10^{-6}$	$1.67219 + i1.24808 \times 10^{-6}$
20	1×10^{-5}	$2.06020 + i1.58950 \times 10^{-6}$	$2.06020 + i1.58948 \times 10^{-6}$	$2.06020 + i1.58936 \times 10^{-6}$
10	1×10^{-2}	$1.67219 + i1.24810 \times 10^{-3}$	$1.67213 + i1.24772 \times 10^{-3}$	$1.67213 + i1.24772 \times 10^{-3}$
20	1×10^{-2}	$2.06020 + i1.58950 \times 10^{-3}$	$2.06008 + i1.58907 \times 10^{-3}$	$2.06008 + i1.58907 \times 10^{-3}$

$Re = 10$, $r_2 = 1$, $\epsilon = 1$, $F = S = 0$, $n_1 = n_2 = 1$.

routine that implements the QZ algorithm. The calculations were performed in double-precision arithmetic on an IBM 6000 workstation. In forming stability maps, up to $N = 20$ terms for Newtonian fluids and up to $N = 50$ terms for shear-rate-dependent-viscosity liquids were used to achieve convergence in the computation of eigenvalues.

The choice of collocation points, or the way of transforming the physical domain $-\epsilon \le y \le 1$ to the spectral domain $-1 \le Y \le 1$ has a dramatic effect on convergence. Transformation of $-\epsilon \le y \le 1$ to $-1 \le Y \le 1$ ($Y = \epsilon_1$, where $\epsilon_1 = (\epsilon - 1)/(\epsilon + 1)$, corresponds to the fluid–fluid interface) was compared to transforming each of the $0 \le y \le 1$ and $-\epsilon \le y \le 0$ subdomains to separate $-1 \le Y \le 1$ subdomains. The convergence in the latter case is clearly superior. A detailed discussion of the numerical aspects of the algorithm is given by Pinarbasi and Liakopoulos [25].

The computer inplementation of the numerical procedure outlined above was tested by comparing the computed results with asymptotic results reported by Yih [4], and Su and Khomami [18]. As a first test, both CY and BL model fluids should reduce to Newtonian fluids for $n_1 = n_2 = 1$ (for CY fluids) and $\tau_{y1} = \tau_{y2} = 0$ (for BL fluids). The results of this test are summarized in Table 1. The agreement is excellent for small values of α, but the results deviate slightly as α increases since the asymptotic analysis is valid for $\alpha \to 0$. As a second test, the eigenvalues computed numerically using our code were compared with the asymptotic results of Su and Khomami [18] for power-law fluids. The stability maps for power-law fluids are given in Pinarbasi and Liakopoulos [27]. Representative results of this test are given in Table 2. The agreement is excellent.

Table 2
Comparison of asymptotic and numerical results for two power-law fluids

n_1	n_2	Asymptotic (Su and Khomami [18])	Numerical (present study)
0.5	1.0	$1.1867 + i1.6617 \times 10^{-5}$	$1.1866 + i1.6614 \times 10^{-5}$
0.75	1.0	$1.1236 + i8.5941 \times 10^{-6}$	$1.1236 + i8.5933 \times 10^{-6}$
0.35	1.0	$1.2170 + i2.1434 \times 10^{-5}$	$1.2170 + i2.1429 \times 10^{-5}$

$Re = 0.1$, $\alpha = 10^{-2}$, $m_2 = 0.5$, $r_2 = 1$, $F = S = 0$, $\epsilon = 1.0$.

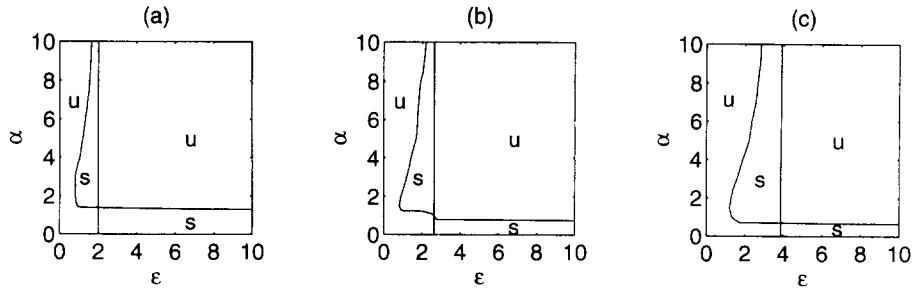

Fig. 2. Stability maps of Newtonian/Bingham-like fluids. (a) $\tau_{y1} = \tau_{y2} = 0$; (b) $\tau_{y1} = 0$, $\tau_{y2} = h_2 = 2$; (c) $\tau_{y1} = 0$, $\tau_{y2} = h_2 = 4$. ($Re = 0.1$, $F = S = 0$, $r_2 = 1$, $m_2 = 4$; S, stable; U, unstable.)

4. Results and discussion

4.1. Bingham-like fluids

A plastic material exhibits little or no deformation up to a certain level of stress, called the yield stress and flows like a fluid when the stress level exceeds the yield stress. The standard Bingham model is a well-known, one-parmeter constitutive law for an ideal viscoplastic material that models adequately the stress–strain rate relation for many pastes and fine suspensions. However, the standard Bingham model requires the tracking of material yield surfaces. The constitutive model used in our analysis, Eq. (8), was proposed by Papanastasiou [22] for Bingham-like materials with yield, where a material parameter controls the exponential growth of stress. The model is valid for both yielded and unyielded areas. Therefore, tracking of material yield surfaces is not required. Another main feature of this model is that it mimics the ideal Bingham plastic for relatively large stress growth exponents.

Fig. 2(a) shows the stability map of two superposed Newtonian fluids for $Re = 0.1$, $F = S = 0$, $r_2 = 1$, and $m_2 = 4$. This figure, obtained as a special case of the Bingham-like formulation by setting $\tau_{y1} = \tau_{y2} = 0$, is included here for comparison with the stability characteristics of Bingham-like fluids. Stability maps for a flow system consisting of a Bingham-like fluid (bottom layer, fluid 2) and a Newtonian fluid (upper layer, fluid 1) are presented in Figs. 2(b) and 2(c). The values of Re, F, S, r_2 and m_2 are as in Fig. 2(a), while $h_2 = \tau_{y2} = 2$ in Fig. 2(b), and $h_2 = \tau_{y2} = 4$ in Fig. 2(c). There exists a straight line, corresponding to a constant thickness ratio, along which the flow is neutrally stable for all wavenumbers. This neutral stability line occurs at $\epsilon_{cr} = (m_2)^{0.5}$ for a Newtonian fluid and it will be referred to as critical thickness ratio ϵ_{cr}. This line identifies the thickness ratio for which the slope of the base flow velocity profile is continuous across the fluid–fluid interface. Replacing the Newtonian fluid flowing at the bottom layer with a Bingham-like fluid results in shifting ϵ_{cr} to the right (see Figs. 2(b) and 2(c)). This shifting is much more pronounced as the values of h and τ_y are increased. In addition, Fig. 2 shows the overall stabilizing effect of replacing the bottom layer Newtonian fluid with a Bingham-like fluid and increasing its parameters h and τ_y. This stabilizing effect is

observed at intermediate and large wavenumbers which coincide with the stable regions located at $\epsilon < \epsilon_{cr}$. However, the stable region at small wavenumbers, which coincide with the stable region to the right of ϵ_{cr}, becomes smaller as h and τ_y increase.

The effect of stress growth exponent h on the flow stability is shown in Fig. 3. The values of the parameters $Re = 0.1$, $F = S = 0$, $r_2 = 1$, $m_2 = 4$ and $\tau_{y_1} = \tau_{y_2} = 0.5$ are kept fixed while the stress growth exponent of each layer takes the values $h_1 = h_2 = 0.5$ in Fig. 3(a), $h_1 = h_2 = 1$ in Fig. 3(b), and $h_1 = h_2 = 1.5$ in Fig. 3(c). Increasing the stress growth exponent of the fluids stabilizes the flow. This stabilizing effect is observed in the regions to the left of ϵ_{cr}. In this region, where wavenumbers are small, the unstable region vanishes gradually as the stress growth exponent increases. Note that no shifting of ϵ_{cr} occurs as h increases.

The effect of yield stress τ_y on the interfacial stability is presented in Fig. 4. The fixed parameters for this case are $Re = 0.1$, $F = S = 0$, $r_2 = 1$, $m_2 = 4$ and $h_1 = h_2 = 0.5$. The yield stress is set to $\tau_{y_1} = \tau_{y_2} = 0.5$ in Fig. 4(a), $\tau_{y_1} = \tau_{y_2} = 2$ in Fig. 4(b) and $\tau_{y_1} = \tau_{y_2} = 4$ in Fig. 4(c). Increasing τ_y of the fluids stabilizes the flow especially in the regions to the left of ϵ_{cr}. A comparison of Fig. 4 with Fig. 3 shows

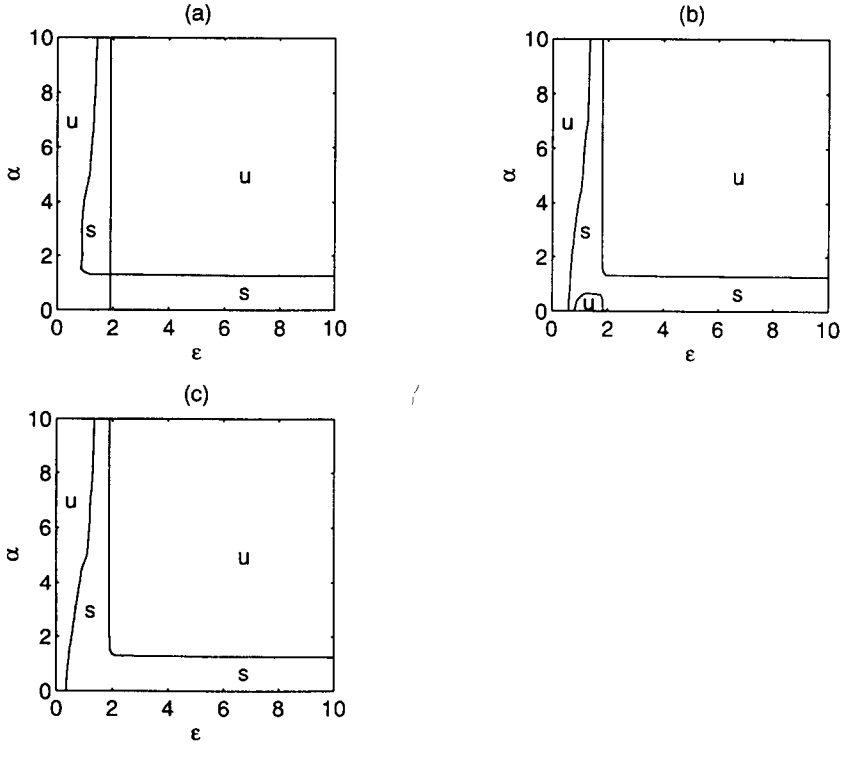

Fig. 3. Stability maps of two Bingham-like fluids for various values of h. (a) $h_1 = h_2 = 0.5$; (b) $h_1 = h_2 = 1.0$; (c) $h_1 = h_2 = 1.5$. ($Re = 0.1$, $F = S = 0$, $r_2 = 1$, $m_2 = 4$, $\tau_{y_1} = \tau_{y_2} = 0.5$; S, stable; U, unstable.)

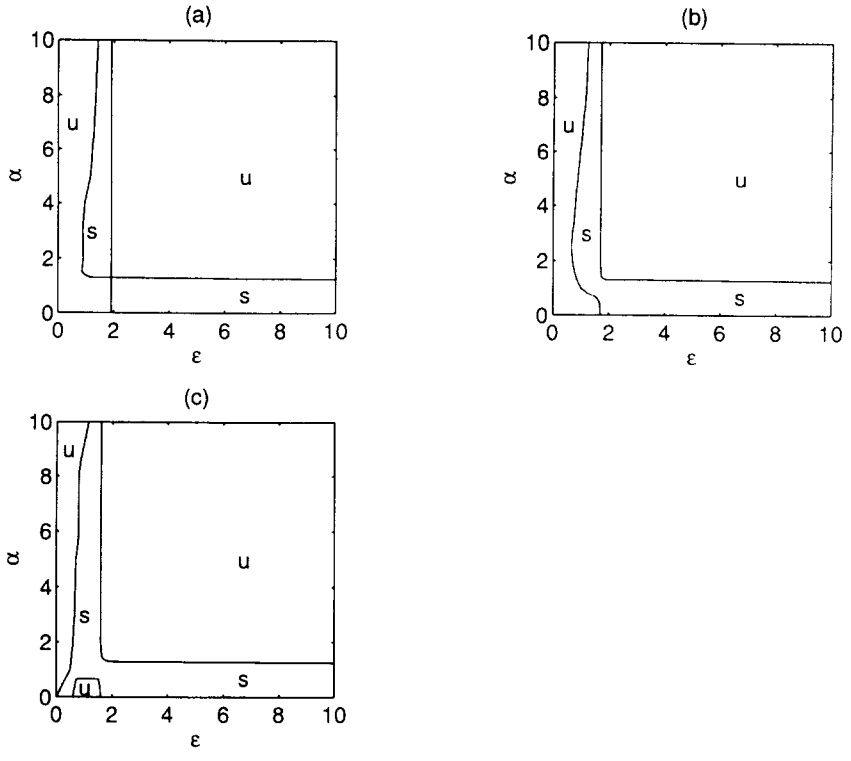

Fig. 4. Stability maps of two Bingham-like fluids for various values of τ_y. (a) $\tau_{y_1} = \tau_{y_2} = 0.5$; (b) $\tau_{y_1} = \tau_{y_2} = 2.0$; (c) $\tau_{y_1} = \tau_{y_2} = 4.0$. ($Re = 0.1$, $F = S = 0$, $r_2 = 1$, $m_2 = 4$, $h_1 = h_2 = 0.5$; S, stable; U, unstable.)

that increasing h and increasing τ_y have similar effects on the stability maps. Note also that ϵ_{cr} shifts slightly to the left as τ_y increases. Frigaard et al. [28] studied recently the stability of single-layer Poiseuille flow of an ideal Bingham fluid. They report that increasing the yield stress has a stabilizing effect on the flow, a trend that is also observed in the present study of two-layer Poiseuille flow using the Bingham-like rheological model.

Fig. 5 shows the effect of zero-shear-rate viscosity ratio m_2 on the interfacial stability of two Bingham-like fluids. The fixed parameters are $Re = 0.1$, $F = S = 0$, $r_2 = 1$, $h_1 = h_2 = 0.5$ and $\tau_{y_1} = \tau_{y_2} = 0.5$, while $m_2 = 4$, 10, 20 in Figs. 5(a), 5(b) and 5(c), respectively. Increasing the zero-shear-rate viscosity ratio causes the stability boundary corresponding to the critical depth ratio, ϵ_{cr}, to shift to the right. In addition, increasing m_2 causes an enlargement of the stable region to the left of ϵ_{cr} and therefore stabilizes the flow in this region. However, increasing m_2 decreases the size of the stable region to the right of ϵ_{cr} where the wavenumbers are relatively small.

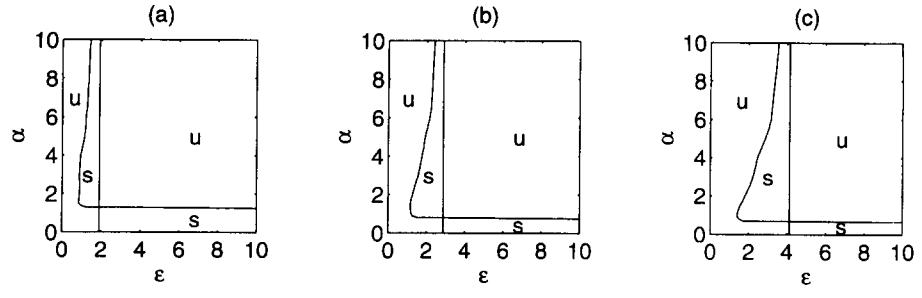

Fig. 5. Stability maps of two Bingham-like fluids for various values of m_2. (a) $m_2 = 4$; (b) $m_2 = 10$; (c) $m_2 = 20$. ($Re = 0.1$, $F = S = 0$, $r_2 = 1$, $\tau_{y1} = \tau_{y2} = 0.5$, $h_1 = h_2 = 0.5$; S, stable; U, unstable.)

4.2. Carreau–Yasuda fluids

The Carreau–Yasuda model has sufficient flexibility to fit a wide variety of experimental viscosity/rate of strain curves [21]. Its predictions depend on the material time constant $\bar{\lambda}$, which signifies the onset of shear thinning, the dimensionless power-law index n, which shows the degree of shear thinning, and the dimensionless Yasuda constant a that describes the transition region between the zero-shear-rate region and the power-law region. It has been shown that good fits can be obtained with $a = 2$ for many concentrated polymer solutions and melts [21]. For $a = 2$, the Carreau–Yasuda model is referred to as the Carreau equation since the parameter a was added later by Yasuda [29] as an independent parameter.

The effect of power-law index n on the flow stability is shown in Fig. 6. Figs. 6(a), 6(b) and 6(c) depict the stability maps for $n_1 = n_2 = 1$, $n_1 = n_2 = 0.5$, and $n_1 = n_2 = 0.25$ respectively. The remaining flow parameters take the values $Re = 0.1$, $F = S = 0$, $r_2 = 1$, $m_2 = 20$. $\lambda_1 = \lambda_2 = 1$ and $a_1 = a_2 = 3$. Our results indicate that, when the extent of shear thinning for each layer is the same, the critical depth ratio increases (the line $\epsilon = \epsilon_{cr}$ shifts to the right) as n is gradually decreased. In addition, as one can see in Fig. 6, decreasing n destabilizes the interface. Since shear thinning increases as the power-law index n decreases, an increase in shear thinning results in more unstable interfaces.

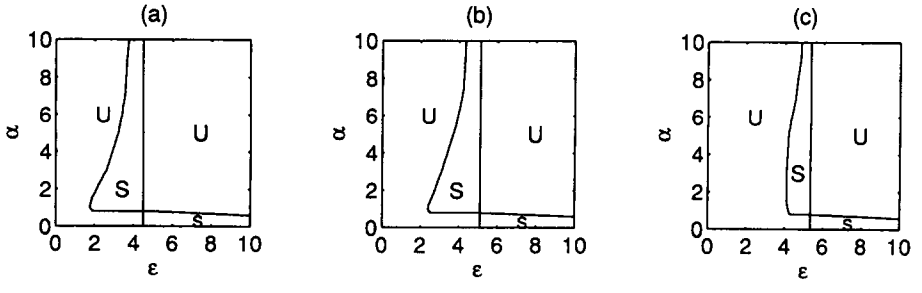

Fig. 6. Stability maps of two Carreau–Yasuda fluids for various values of n. (a) $n_1 = n_2 = 1.0$; (b) $n_1 = n_2 = 0.5$; (c) $n_1 = n_2 = 0.25$. ($Re = 0.1$, $F = S = 0$, $r_2 = 1$, $m_2 = 20$, $\lambda_1 = \lambda_2 = 1$, $a_1 = a_2 = 3$; S, stable; U, unstable.)

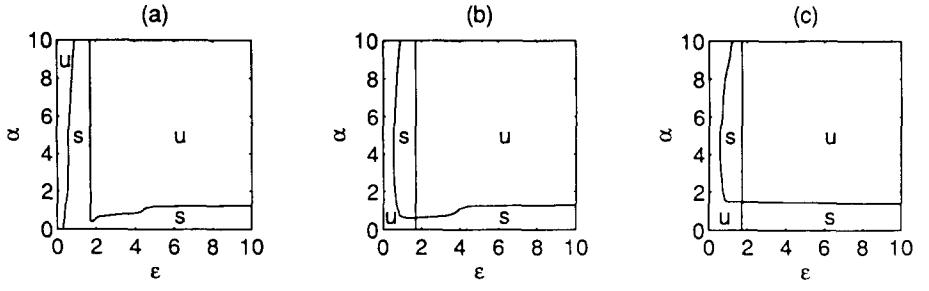

Fig. 7. Stability maps of two Carreau–Yasuda fluids for various values of a. (a) $a_1 = a_2 = 1$; (b) $a_1 = a_2 = 1.25$; (c) $a_1 = a_2 = 3$. ($Re = 0.1$, $F = S = 0$, $r_2 = 1$, $m_2 = 2$, $\lambda_1 = \lambda_2 = 1$, $n_1 = n_2 = 0.25$; S, stable; U, unstable.)

Fig. 7 summarizes the effect of dimensionless constant a on the stability of the interface. The fixed parameters are $Re = 0.1$, $F = S = 0$, $r_2 = 1$, $m_2 = 2$, $\lambda_1 = \lambda_2 = 1$ and $n_1 = n_2 = 0.25$, while $a_1 = a_2 = 1$ in Fig. 7(a), $a_1 = a_2 = 1.25$ in Fig. 7(b), and $a_1 = a_2 = 3$ in Fig. 7(c). No shifting of ϵ_{cr} is observed as the parameter a is gradually increased. Increasing a has a destabilizing effect in the region $\epsilon < \epsilon_{cr}$ and a slight stabilizing effect in the region $\epsilon > \epsilon_{cr}$. The stability maps for $a_1 = a_2 = 2$ (Carreau model) and $a_1 = a_2 = 3$ are practically indistinguishable.

The stability maps of two Carreau–Yasuda fluids at various $\lambda = \lambda_1 = \lambda_2$ are plotted in Fig. 8. The material time constants of the fluids are $\lambda_1 = \lambda_2 = 0$ in Fig. 8(a), $\lambda_1 = \lambda_2 = 2$ in Fig. 8(b) and $\lambda_1 = \lambda_2 = 4$ in Fig. 8(c). Other flow parameters are $Re = 0.1$, $F = S = 0$, $r_2 = 1$, $m_2 = 20$, $n_1 = n_2 = 0.5$ and $a_1 = a_2 = 3$. The critical depth ratio ϵ_{cr} shifts to the right as λ gradually increases. The effect of increasing λ on the stability maps varies from region to region: it has a stabilizing effect on the region to the left of ϵ_{cr} while it destabilizes the region to the right of ϵ_{cr}.

Finally, the stability maps for various m_2 values are presented in Fig. 9. They depict the effect of zero-shear-rate viscosity ratio on the flow stability. The fixed parameters are $Re = 0.1$, $F = S = 0$, $r_2 = 1$, $n_1 = n_2 = 0.25$, $a_1 = a_2 = 3$ and $\lambda_1 = \lambda_2 = 1$, while m_2 is gradually increased: $m_2 = 2$ in Fig. 9(a), 10 in Fig. 9(b), and 20 in Fig. 9(c). Similar to the effect of decreasing n or increasing λ, increasing m_2 causes

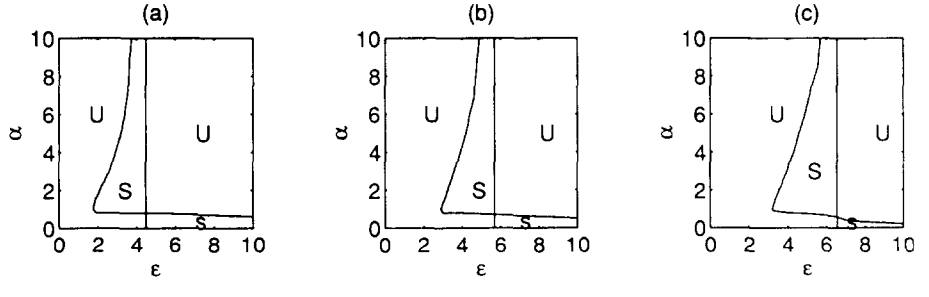

Fig. 8. Stability maps of two Carreau–Yasuda fluids for various values of λ. (a) $\lambda_1 = \lambda_2 = 0$; (b) $\lambda_1 = \lambda_2 = 2$; (c) $\lambda_1 = \lambda_2 = 4$. ($Re = 0.1$, $F = S = 0$, $r_2 = 1$, $m_2 = 20$, $n_1 = n_2 = 0.5$, $a_1 = a_2 = 3$; S, stable; U, unstable.)

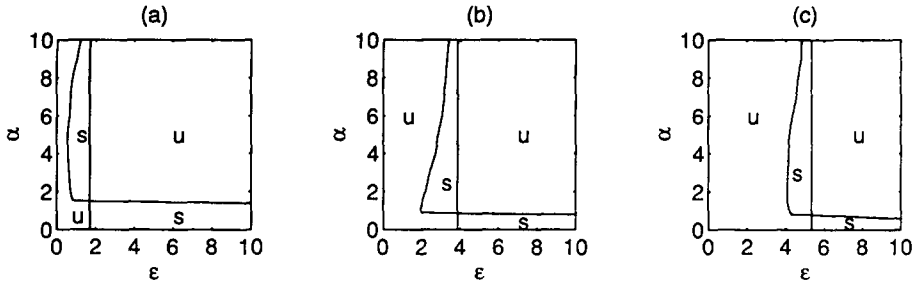

Fig. 9. Stability maps of two Carreau–Yasuda fluids for various values of m_2. (a) $m_2 = 2$; (b) $m_2 = 10$; (c) $m_2 = 20$. ($Re = 0.1$, $F = S = 0$, $r_2 = 1$, $\lambda_1 = \lambda_2 = 1$, $a_1 = a_2 = 3$, $n_1 = n_2 = 0.25$; S, stable; U, unstable.)

the critical depth ratio ϵ_{cr} to shift to the right. However, the effect of increasing m_2 is clearly more pronounced. Fig. 9 shows that increasing m_2 has a destabilizing effect on the fluid–fluid interface for all wavenumbers.

5. Conclusions

A linear stability analysis of two-layer plane Poiseuille flow of inelastic fluids to two-dimensional disturbances has been presented. The constitutive relations considered are the Carreau–Yasuda and Bingham-like models. Stability maps have been presented in the α–ϵ plane for $0.1 \leq \alpha \leq 10$ and $0.1 \leq \epsilon \leq 10$.

Starting with a two-layer Newtonian fluid flow, we have shown that replacing the bottom Newtonian fluid with a viscoplastic fluid has a stabilizing effect on the fluid–fluid interface for intermediate and large wavenumbers.

In the case of two viscoplastic fluids, increasing the stress growth exponent h or increasing the yield stress τ_{y_1} of the fluids has a stabilizing effect on the fluid–fluid interface. In addition, the effect of zero-shear-rate viscosity ratio m_2 can be stabilizing or destabilizing depending on the flow configuration and wavelength.

In the case of two shear thinning fluids, we have shown that an increase in shear thinning or zero-shear-rate viscosity ratio destabilizes the flow. Furthermore, the effect of variations in the onset of shear thinning or Yasuda constant a can be stabilizing or destabilizing depending upon the wavelength and the layer thickness ratio.

Acknowledgment

This work was partially supported by NSF, under grant No. DDM-9110850.

References

[1] M.E. Charles and L.U. Lilleleht, J. Fluid Mech., 22 (1965) 217.
[2] H.S. Yu and E.M. Sparrow, Trans. ASME, J. Heat Transfer, 91 (1969) 51.

[3] T.W. Kao and C. Park, J. Fluid Mech., 52 (1972) 401.
[4] C.S. Yih, J. Fluid Mech., 27 (1967) 337.
[5] C.E. Hickox, Phys. Fluids, 14 (1971) 251.
[6] C. Nakaya and E. Hasegawa, J. Phys. Soc. Jpn., 37 (1974) 214.
[7] A.P. Hooper and W.G.C. Boyd, J. Fluid Mech., 128 (1983) 507.
[8] A.P. Hooper and R. Grimshaw, Phys. Fluids, 28 (1985) 37.
[9] Y. Renardy, Phys. Fluids, 28 (1985) 3441.
[10] Y. Renardy, Phys. Fluids, 30 (1987) 1627.
[11] Y. Renardy, Phys. Fluids A, 1 (1989) 1666.
[12] S.G. Yiantsios and B.G. Higgins, Phys. Fluids, 31 (1988) 3225.
[13] C.H. Li, Phys. Fluids, 12 (1969) 531.
[14] N.D. Waters and A.M. Keeley, J. Non-Newtonian Fluid Mech., 24 (1987) 161.
[15] Y. Renardy, J. Non-Newtonian Fluid Mech., 28 (1988) 99.
[16] A.A. Khan and C.D. Han, Trans. Soc. Rheol., 20 (1976) 595.
[17] B. Khomami, J. Non-Newtonian Fluid Mech., 36 (1990) 289.
[18] Y.Y. Su and B. Khomami, Chem. Eng. Commun., 109 (1991) 209.
[19] Y.Y. Su and B. Khomami, J. Rheol., 36 (1992) 357.
[20] N.R. Anturkar, T.C. Papanastasiou and J.O. Wilkes, AIChE J., 36 (1990) 710.
[21] R.B. Bird, R.C. Armstrong and O. Hassager, Dynamics of Polymeric Liquids, vol. 1, Fluid Mechanics, Wiley, New York, 1987.
[22] T.C. Papanastasiou, J. Rheol., 31 (1987) 385.
[23] S.A. Orszag, J. Fluid Mech., 50 (1971) 689.
[24] D. Gottlieb and S.A. Orszag, Numerical Analysis of Spectral Methods: Theory and Applications, CBSM-NSF Regional Conference Ser. Appl. Math., 26, SIAM, Philadelphia, 1977.
[25] A. Pinarbasi and A. Liakopoulos, Technical Report, Lehigh University, Bethlehem, PA, 1994.
[26] P.G. Drazin and W.H. Reid, Hydrodynamic Stability, Cambridge University Press, Cambridge, MA, 1981.
[27] A. Pinarbasi and A. Liakopoulos, ASME, HTD, 259 (1993) 113.
[28] I.A. Frigaard, S.D. Howison and I.J. Sobey, J. Fluid Mech., 263 (1994) 133.
[29] K. Yasuda, Ph.D. Thesis, MIT, Cambridge, MA, 1979.